Research Square

Preprints are preliminary reports that have not undergone peer review.
They should not be considered conclusive, used to inform clinical practice,
or referenced by the media as validated information.

Flattened yarn path point modeling method for complex 3D woven composites

Yinping Ye
Donghua university
Chengchang Ji
Donghua university
Xinfu Chi
xinfu.chi@dhu.edu.cn
Donghua university
Yize Sun
Donghua university

Research Article

Keywords: 3D weaving, yarn path points, complex structures, thickness distribution

Posted Date: March 16th, 2026

DOI: https://doi.org/10.21203/rs.3.rs-9040628/v1

License: This work is licensed under a Creative Commons Attribution 4.0 International License.
Read Full License

Additional Declarations: No competing interests reported.

Flattened yarn path point modeling method for complex 3D woven composites

Yinping Ye, Chengchang Ji*, Xinfu Chi*, Yize Sun

College of Mechanical Engineering, Donghua University, 2999 Renmin North Road, Songjiang District, Shanghai, China.

*Corresponding author. Email: jicc@dhu.edu.cn (C. Ji), xinfu.chi@dhu.edu.cn(X. Chi)

Abstract:To address challenges in accurately characterizing yarn paths and extracting thickness distributions for complex 3D woven composites in digital manufacturing, this paper proposes a parametric extraction method for yarn path points in the flattened state. First, the initial STL model is segmented along the warp direction according to weft width. Cross-sectional boundary points are extracted and interpolated clockwise to precisely partition each cross-sectional area. Then, a classification criterion is established to identify cross-sectional types, and a differentiated layering method is applied to extract initial yarn path points along the thickness direction. A flattening reference line is then determined using an algorithm adapted to each cross-sectional type. Finally, each layered cross-section is flattened based on this reference line, enabling the reconstruction of a 3D woven yarn path point model. The method was validated using 3D woven composite models with various structures and process parameters. Results demonstrate that the proposed approach accurately reconstructs yarn path points of complex preforms in the flattened state and accommodates diverse processing conditions, offering critical support for the digital design and manufacturing of 3D woven composites.

Highlights:

(1) Automatically extract flattened yarn path point model of 3D woven composites.

(2) Adapt to composite models with different process parameters and structures.

(3) Automatically extract thickness distribution of complex 3D woven composites.

Keywords: 3D weaving; yarn path points; complex structures; thickness distribution

1. Introduction

3D weaving is an important technology in composite manufacturing, which can perfectly combine strength [1, 2], durability [3], and structural integrity [4, 5]. It is mainly applied in aerospace, marine, and automotive fields, with typical products including aero-engine blades, tail fins, and automotive leaf springs [6-8]. The performance of the final product, such as yarn volume fraction, organizational structure [9, 10], and near-net shape accuracy [11], is determined by the design parameters during the weaving process. However, 3D woven components such as aero-engine blades have complex geometric structures, making it difficult to extract process design parameters. With the development of industrial manufacturing technology, computer-aided design/manufacturing (CAD/CAM) technology plays a crucial role in the accurate and rapid extraction of component process parameters. Accurate thickness decomposition technology can help optimize design parameters to realize the near-net shape design of complex structures.

3D woven preforms inevitably undergo torsion and compression deformation during the molding process [12-14]. Due to the combined effect of multiple forces, this undoubtedly increases the complexity of the inverse solution design of 3D woven composite structures. Mechanical models of yarn composites are constructed by mechanical methods, and finite element methods are used to simulate the deformation of woven preforms. Both 2D [15-17] and 3D [18-20] woven yarn material forming simulation methods

have been studied. Mesoscale simulation determines the performance of textile composites, and mesoscopic finite elements are highly dependent on the initial geometry. Naouar et al. [21] proposed a real geometric modeling method based on μCT, which can accurately characterize the fiber direction, avoid interpenetration, and achieve better results than traditional modeling. Li et al. [22] established a numerical modeling method considering real yarn geometry, generating high-fidelity geometry through digital element analysis and reconstruction algorithms, accurately characterizing fiber orientation. Combined with hyperelastic models and Micro-CT experimental verification, it has high simulation accuracy and can be used for composite design and structural optimization. Thompson et al. [23] established a numerical modeling method for the kinematic behavior of non-crimp fabrics (NCF), accurately depicting the interaction between tows and stitching yarns. It can directly predict macro responses and extract internal structures from mesoscale effects, effectively characterize local and global deformations, and agree well with experimental results. Sirtautas et al. [24] proposed a mesoscale modeling method for NCF drapability, which can characterize tow and stitch deformation and their interactions. It adopts coarse modeling to adapt to the structural scale, and realizes coupled draping and infusion simulation combined with experimental data, with good verification results for hemispherical parts.

Although mesoscopic and microscopic simulations can accurately characterize yarn details, the calculation of a large number of yarn contacts leads to low efficiency. Therefore, multi-scale simulation has gradually been introduced into related research. The meso-macro forming analysis proposed by Wang et al. [25] can effectively control the calculation cost and provide a foundation for engineering applications, but it still has limitations in yarn elongation prediction. The layered multi-scale method has been successfully applied in the mechanical performance analysis of composites [26, 27], and Li et al. [28] further applied it to the mesoscopic geometric simulation of 3D woven reinforcements, and first introduced an anisotropic hyperelastic constitutive model in macro fabric forming. However, affected by factors such as differences in scale effects and the one-to-one correspondence between woven structures and constitutive models, the existing methods have insufficient versatility and are difficult to meet engineering needs. In addition, lightweight modeling also provides ideas for improving simulation efficiency. Gao et al. [29] took the component cross-section as input and constructed a plain weave mesoscopic preform based on a curvilinear coordinate system and a sine model; Morioka et al. [30] proposed a flattening simulation method for constant-thickness 3D structures, which can simultaneously predict material shape and fiber orientation.

In this paper, a parameterized extraction method for the flattened yarn path point model of complex 3D woven composites is proposed. The complex 3D woven composite model is reconstructed to extract its upper and lower surfaces. Then, different layering methods are proposed for different types of cross-sectional areas to improve the adaptability of the layering method. At the same time, considering the mapping effect between adjacent cross-sectional areas, the reference center line for the flattening process of yarn path points is extracted. The reconstructed 3D woven yarn path point model reflects the torsional deformation of the preform during the forming process of composites with complex geometric shapes, laying a foundation for improving the near-net shape design of 3D woven composites. In addition, the thickness distribution data of composites can be quickly derived from the flattened yarn path point model, which helps to better guide the design and production of 3D woven composites.

2. Construction of Yarn Path Points for 3D Woven Preforms

Extracting yarn path points is essential for the design of complex 3D woven composites, which can

be obtained by segmenting the composite into unit cells and arranging them in sequence. As shown in Fig. 1(b), an interlacing point area is regarded as a rectangular area in this paper, ignoring the influence of binding yarn buckling on the overall length dimension of the preform. The length and width of the rectangular area are the weft width W_{weft} and warp width W_{warp}, respectively, and the height is a multiple of the yarn thickness T_{yarn}. The methods for constructing yarn thickness, width, and yarn path points of 3D woven preforms are described in detail in Sections 2.1 and 2.2.

2.1 Thickness and Width of Yarns

Obtaining yarn thickness, width, and thickness parameters is crucial for constructing accurate 3D woven yarn path points, which can be obtained by observing the composite cross-section [29] and measuring the warp density and weft density of the fabric surface, respectively. As shown in Figs. 1(d) and (h), they are the cross-section of the woven composite and the surface of the fabric observed by an electron microscope, respectively.

The drag centerline of the weft yarn shown in Fig. 1(e) can be regarded as a sine wave in the curvilinear coordinate system. As shown in Fig. 1(f), the profiles of the three yarn cross-sections are convex at both the top and bottom. Since the warp tows and weft tows are in contact at their wave crests and troughs, the cross-sectional shape of the warp tows can be determined by the shape of the warp centerline at the contact positions. The data at position 3 in each yarn cross-section is shown in Fig. 1(g), which is the maximum thickness in the cross-sectional shape of the warp yarn, and the average value of the measured data is used as the support for the thickness data when constructing the yarn path point model.

$$W_{warp} = \frac{10}{\sigma_{warp}} \tag{1}$$

$$W_{weft} = \frac{10}{\sigma_{weft}} \tag{2}$$

As shown in Eqs. (1)-(2), σ_{warp} and σ_{weft} are the warp density and weft density, respectively, which are important parameters in the weaving process. They represent the number of yarns (warp and weft) per centimeter, and the warp width W_{warp} and weft width W_{warp} of the preform can be accurately calculated through these process parameters.

2.2 Yarn Path Points of 3D Woven Preforms

3D woven preforms are formed by the interlacing of warp yarns, weft yarns, and binding yarns, and the yarn path points of the preforms are distributed in a staggered manner. In this paper, the thickness of the composite is taken as the reference for the reconstruction of yarn path points, and the lower surface is regarded as the starting surface in the process of constructing yarn path points. As shown in Fig. 1(a), the thickness of the woven composite is $T_{composite}$, the length along the weft direction is L_{weft}, and the length along the warp direction is L_{warp}. The overall point set of initial yarn path points is $S_{initial}=\{P_{(i,j,k)}|i=1,\ldots,m,j=1,\ldots,n,k=1,\ldots,h\}$. As shown in Fig. 1(c), there are $m(P_{(j,k)})$ yarn path points in thej-th row and k-th layer, $n(P_{(j,k)})$ yarn path points in the o-th column and k-th layer, and $h(P_{(j,k)})$ yarn path points in the i-th column and j-th row.

$$m(P_{(j,k)}) = \frac{L_{weft}(j,k)}{W_{warp}} \tag{3}$$

$$n(P_{(i,k)}) = \frac{L_{warp}(i,k)}{W_{weft}} \tag{4}$$

$$h(P_{(i,j)}) = \frac{T_{composite}(i,j)}{T_{yarn}} \tag{5}$$

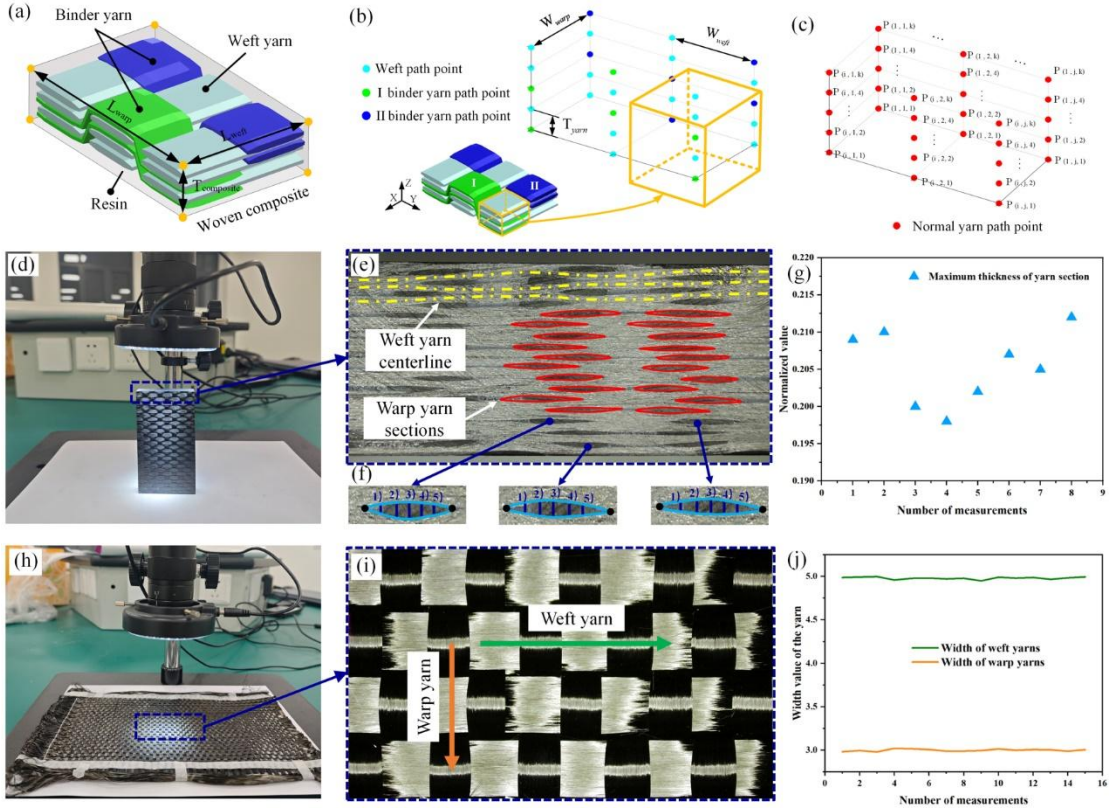


Fig. 1 (a) Geometric model of 3D woven composites; (b) Yarn path points of different yarns; (c) Overall yarn path points. Construction of yarn thickness: (d) and (h) Cross-sectional observation of 3D woven composites; (f) Warp yarn cross-sectional area; (g) Warp yarn thickness measurement data. Construction of yarn width: (h) and (i) Surface observation of 3D woven fabrics; (j) Warp and weft yarn width measurement data.

3. Parameterized Extraction Process of Yarn Path Points in Flattened State

The composites shown in Fig. 1(d) and the woven fabrics in Fig. 1(h) both have regular structures, and the distribution of their yarn path points is easy to obtain. However, taking aero-engine blades as an example, such composite components have complex curvature changes and high requirements for near-net shape design. During the weaving and forming processes, the yarns are twisted, and the thickness of the composite components along the warp and weft directions changes, resulting in difficulty in extracting their yarn path points. Therefore, this paper proposes a parameterized method for extracting the flattened yarn path point model of 3D woven composites to facilitate the accurate design of such composite structures.

Fig. 2 shows the calculation principle diagram of the flattened yarn path point model for complex 3D woven composites. It is mainly divided into four steps: the first step is to segment the initial composite STL model along the warp direction based on the weft width W_{weft} to extract the boundary points of the cross-sectional area, and perform clockwise interpolation on them. The second step is to judge the type

of the cross-sectional area and adopt different layering methods for different types of cross-sectional areas, so as to accurately extract the initial yarn path points along the thickness direction in the cross-sectional area. The third step is to adopt different extraction methods to extract the flattening reference line for different types of cross-sectional areas. The fourth step is to flatten the layered cross-sectional areas based on the flattening reference line, thereby reconstructing the 3D woven yarn path points. The extraction logic diagram of the flattened yarn path point model for complex 3D woven composites is shown in Fig. 3, and each step will be described in detail in Sections 3.1-3.4.

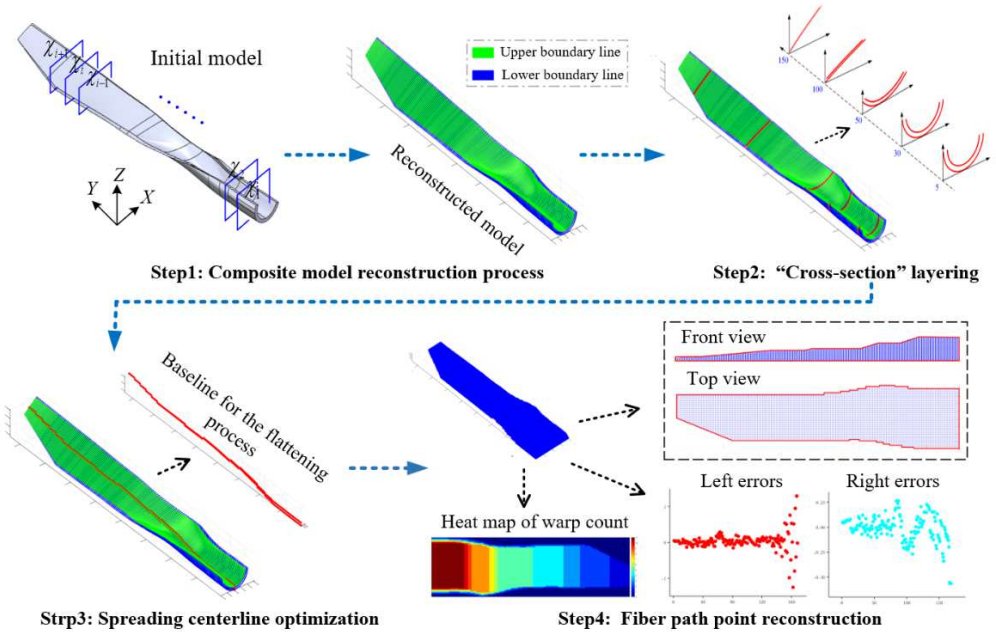


Fig. 2 Calculation principle of the flattened yarn path point model for complex 3D woven composites.

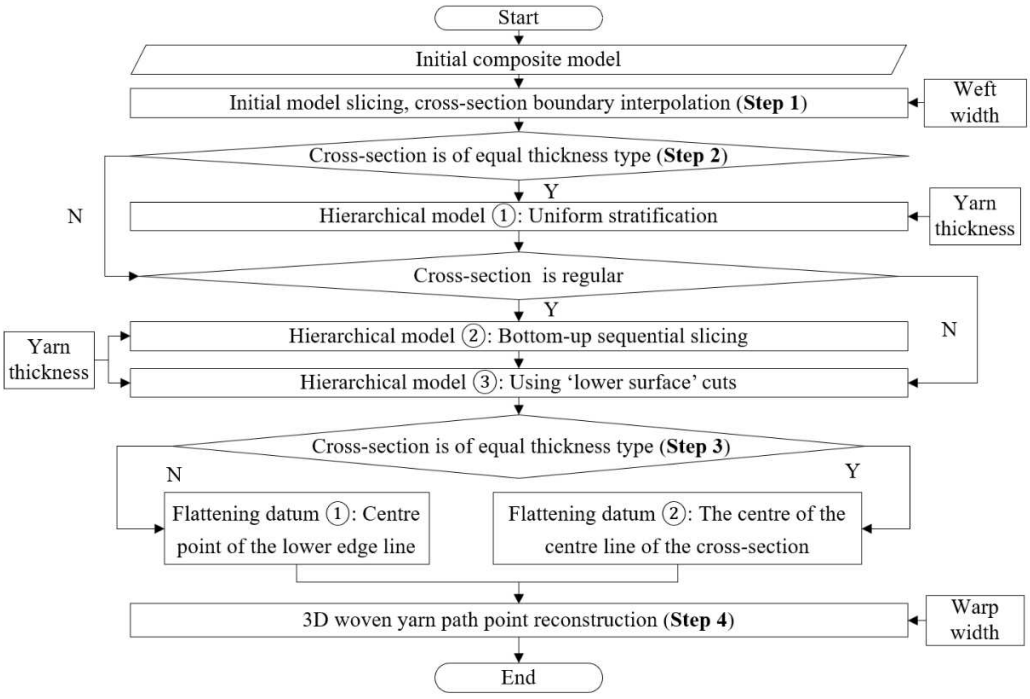


Fig. 3 Logic diagram of the flattened yarn path point model for complex 3D woven composites.

3.1 Reconstruction of Cross-Sectional Area Boundaries

3D woven preforms are formed by the interlacing of warp yarns, weft yarns, and binding yarns, and the size of the interlacing points determines the profiling accuracy of the preforms. To achieve accurate thickness decomposition of the composites, this paper segments the composite component along the warp direction with the weft width as a unit, which is regarded as a component unit of the composite component. The central cross-section of the component unit is extracted as the representative cross-section of the region.

As shown in Fig. 4(a), the initial 3D boundary points α_1 are the set of triangular patch vertices in the triangular patch set α_2 of the STL model. Equidistant interpolation is performed on the two vertices on any edge in the triangular patch set to obtain a dense and uniform 3D model contour point set α_3. The total set of cutting planes is $\beta = \{\chi_j \mid j = 1,\ldots,m_1\}$, where $m_1 = \dfrac{Max(L_{warp}(i,k))}{W_{weft}}$. The intersection points between the cutting plane set χ_j and the 3D model contour point set α_3 are equivalent to the intersection points between the cutting planes χ_j and the boundaries of each triangular patch in the triangular patch set α_2. The initial cross-sectional area boundary point set can be quickly extracted by the above method. The cross-sectional area boundary point set is $S_{\text{cross-section}} = \{S_{\text{cross-section}}(j) \mid j = 1,\ldots,m_1\}$, the point set of a single cross-sectional area is $S_{\text{cross-section}}(j) = \{P_{(g,j)}(u,v) \mid g = 1,\ldots,m_2\}$, and m_2 is the number of boundary point sets in the j-th cross-sectional area.

The points in the initial cross-sectional area boundary point set are unordered. A greedy strategy is used to initialize the initial path of the cross-sectional area, making it a closed and ordered polygon. The Euclidean distance between points is calculated clockwise, and the 2-opt optimization algorithm is used to improve the path to avoid intersections between boundary points. Finally, equidistant interpolation is performed on the point set in the clockwise direction to obtain a uniform and ordered cross-sectional area point set $S'_{\text{cross-section}} = \{S'_{\text{cross-section}}(j) \mid j = 1,\ldots,m_1\}$, where the point set of a single cross-sectional area is $S'_{\text{cross-section}}(j) = \{P'_{(g_1,j)}(u,v) \mid g_1 = 1,\ldots,m_3\}$, and m_3 is the total number of boundary points in the j-th cross-sectional area after sequential interpolation.

Calculate the included angle $\theta\{P'_{(g_1-1,j)}(u,v), P'_{(g_1,j)}(u,v), P'_{(g_1+1,j)}(u,v)\}$ formed between point $P'_{(g_1,j)}(u,v)$ in set $S'_{\text{cross-section}}(j)$ and its adjacent two points, and extract the endpoint set of the cross-sectional area based on the principle of minimum included angle. The endpoints in the cross-sectional area are $\delta(j) = \{P'_{(g_2,j)}(u,v) \mid g_2 = 1,\ldots,m_4\}$, where m_4 is the number of endpoints. The

endpoint set $\delta(j)$ is used to orderly segment the cross-sectional area point set $S'_{\text{cross-section}}(j)$ to obtain the sub-sets $S''_{\text{cross-section}}(j)=\{\varepsilon_{(g_2,j)} \mid g_2=1,\ldots,m_4\}$ of the cross-sectional area, where the number of sub-sets is equal to the number of endpoints. Finally, the upper boundary point set $\varepsilon_{up(g_2,j)}$ and lower boundary point set $\varepsilon_{down(g_2,j)}$ of the cross-sectional area are determined according to the average value of the *x*-values in the sub-sets.

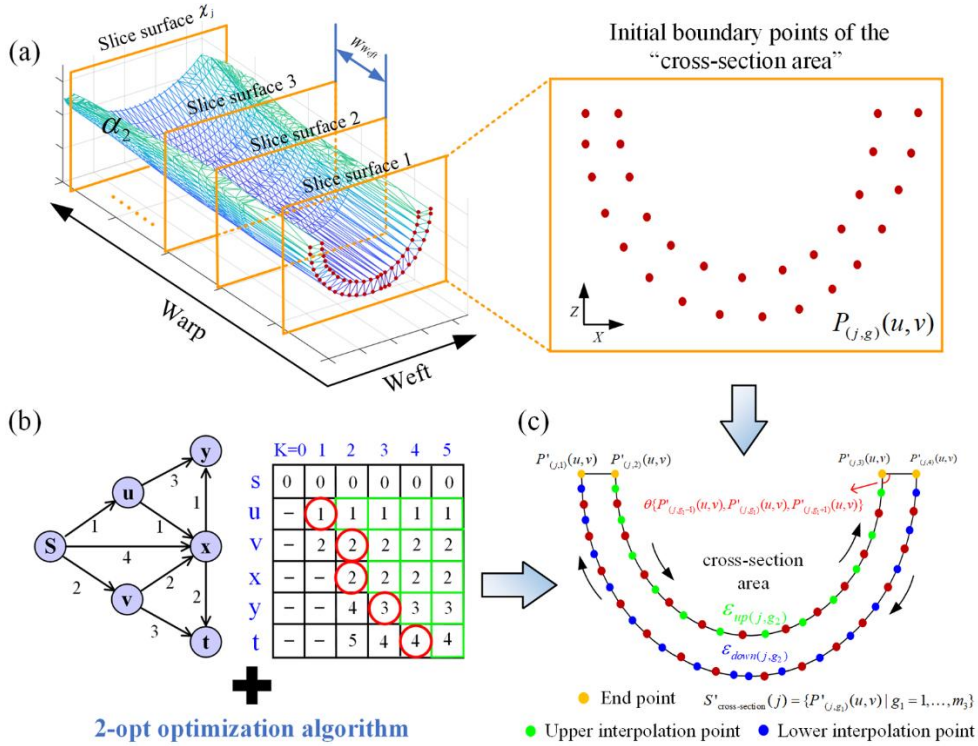


Fig. 4 (a) Extraction of initial boundary points of the cross-sectional area; (b) Extraction of the cross-sectional area path based on the greedy algorithm and 2-opt optimization algorithm; (c) Clockwise interpolation of the cross-sectional area.

3.2 Judgment of Cross-Sectional Area Types and Their Layering Methods

As shown in Fig. 3, judging whether the cross-sectional area is of constant thickness type is a key step, which will be described in detail in Section 3.2.1. It is mainly used to distinguish whether the component is of constant thickness cross-sectional type. Meanwhile, adaptive layering methods are proposed based on the component cross-sectional types, which can be divided into components with constant thickness cross-section, two-boundary cross-section, and regular cross-section types.

3.2.1 Judgment Method of Cross-Sectional Area Types

Calculate the normal vectors $\overrightarrow{F_{ls}}$ and $\overrightarrow{F_{rs}}$ of the boundary endpoints $\zeta'_l(s)$ and $\zeta'_r(s)$ of the short edge line, respectively, and the normal vectors intersect the long edge line at points $\zeta'_l(l)$

and $\zeta'_r(l)$ respectively. As shown in Fig. 6(d), θ_{ls} and θ_{rs} are the included angles formed between the normal vector $\{\overrightarrow{F_{ls}}, \overrightarrow{F_{rs}}\}$ at the endpoints and the positive and negative directions of the u-axis, respectively. θ_f is the optimized included angle to judge the positive and negative values of the slope of the normal vector. The positive and negative values of the slope of the normal vector are consistent with the positive and negative values of $\cos(\theta_f)$, which can be mainly divided into two cases: the short edge line is above the long edge line and the short edge line is below the long edge line. When the short edge line is above the long edge line:

Left endpoint:

$$\begin{cases} \theta_{f1} = \theta_{ls}\{u, \overrightarrow{F_{ls}}\} + 90^\circ, \theta_{ls} \in [0, 90^\circ] \\ \theta_{f2} = \theta_{ls}\{u, \overrightarrow{F_{ls}}\} + 90^\circ, \theta_{ls} \in [90^\circ, 180^\circ] \\ \theta_{f3} = \theta_{ls}\{u, \overrightarrow{F_{ls}}\} + 450^\circ, \theta_{ls} \in [-180^\circ, -90^\circ] \end{cases} \tag{6}$$

Right endpoint:

$$\begin{cases} \theta_{f1} = 270^\circ - \theta_{rs}\{-u, \overrightarrow{F_{rs}}\}, \theta_{rs} \in [90^\circ, 180^\circ] \\ \theta_{f2} = 270^\circ - \theta_{rs}\{-u, \overrightarrow{F_{rs}}\}, \theta_{rs} \in [0, 90^\circ] \\ \theta_{f3} = 270^\circ - \theta_{rs}\{-u, \overrightarrow{F_{rs}}\}, \theta_{rs} \in [-90^\circ, 0] \end{cases} \tag{7}$$

When the short edge line is below the long edge line:

Left endpoint:

$$\begin{cases} \theta_{f1} = 270^\circ - \theta_{ls}\{u, \overrightarrow{F_{ls}}\}, \theta_{ls} \in [-90^\circ, 0] \\ \theta_{f2} = 270^\circ - \theta_{ls}\{u, \overrightarrow{F_{ls}}\}, \theta_{ls} \in [-180^\circ, -90^\circ] \\ \theta_{f3} = 270^\circ - \theta_{ls}\{u, \overrightarrow{F_{ls}}\}, \theta_{ls} \in [90^\circ, 180^\circ] \end{cases} \tag{8}$$

Right endpoint:

$$\begin{cases} \theta_{f1} = \theta_{rs}\{-u, \overrightarrow{F_{rs}}\} + 270^\circ, \theta_{rs} \in [-180^\circ, -90^\circ] \\ \theta_{f2} = \theta_{rs}\{-u, \overrightarrow{F_{rs}}\} + 270^\circ, \theta_{rs} \in [-90^\circ, 0] \\ \theta_{f3} = \theta_{rs}\{-u, \overrightarrow{F_{rs}}\} + 270^\circ, \theta_{rs} \in [0, 90^\circ] \end{cases} \tag{9}$$

Based on the principle of equal adjacent distances, the point sets $\phi(s) = \{\zeta'_r(s), P'_{i_1} \mid i_1 = 1, \ldots, m_5, \zeta'_l(s)\}$ and $\phi(l) = \{\zeta'_r(l), P'_{i_2} \mid i_2 = 1, \ldots, m_5, \zeta'_l(l)\}$ of the short edge line $\zeta'_l(s)\ \zeta'_r(s)$ and the long edge line $\zeta'_l(l)\ \zeta'_r(l)$ are extracted respectively. Among them, the point sets $\phi(s)$ and $\phi(l)$ need to satisfy: $L\{P'_{i_1-1}, P'_{i_1}\} = L\{P'_{i_1}, P'_{i_1+1}\}$, $L\{P'_{i_2-1}, P'_{i_2}\} = L\{P'_{i_2}, P'_{i_2+1}\}$. As shown in Fig. 5(a), the distances $\varphi(j) = \{L_{(i_3,j)} \mid i_3 = 1, \ldots, m_5\}$ between the corresponding points in the $i_1(i_2)$-th group of $\phi(s)$

and $\phi(l)$ are calculated. Fig. 5(b) shows the thickness distribution of the cross-sectional area when j=30. As shown in Fig. 5(c), when all the thickness extreme differences in $j=1,\ldots,m$ are less than T_{yarn}, the cross-sectional area is judged as a constant thickness cross-section.

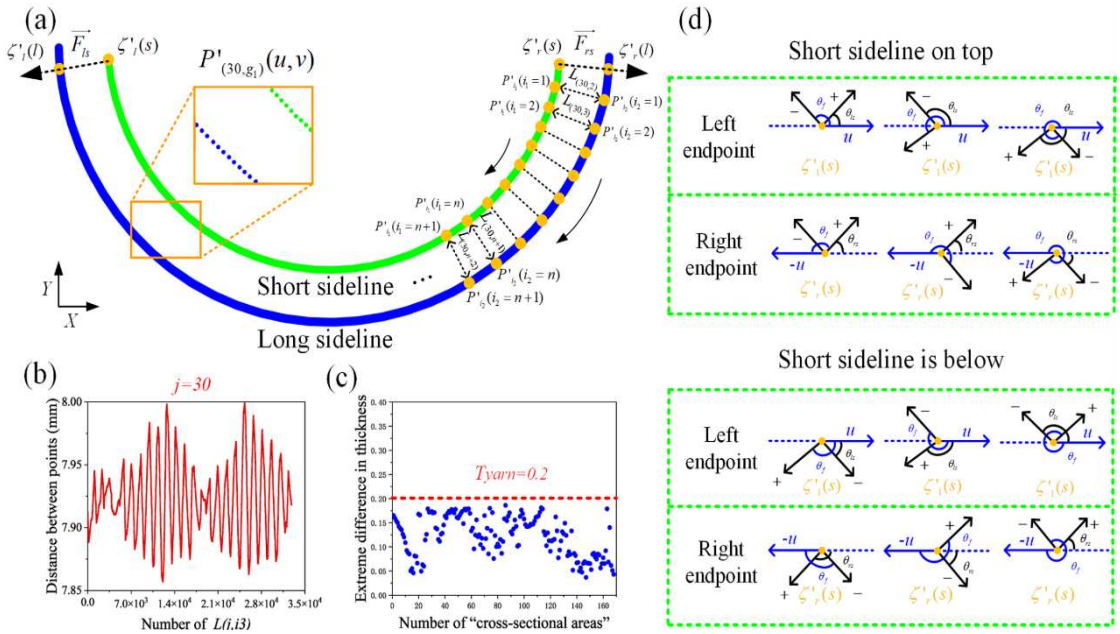


Fig. 5 Judgment method of constant thickness cross-sectional area type: (a) Extraction of thickness data of the cross-sectional area; (b) Thickness of a single cross-sectional area; (c) Thickness range distribution of all cross-sectional areas; (d) Principle for judging the positive and negative values of the slope of the normal vectors at the left and right endpoints of the short edge line.

3.2.2 Layering Method of Cross-Sectional Areas

For the constant thickness cross-sectional area shown in Fig. 6(a), the number of cutting layers is $\eta_j = \dfrac{mean(\varphi(j))}{T_{yarn}}$, where $mean(\varphi(j)) = \dfrac{\sum_{i_3,j}^{i_3=m_5} L_{(i_3,j)}}{m_5}$. As shown in Fig. 6, the cross-sectional area is evenly divided into edge line sets $\lambda(j)$ and $\lambda(j)=\{\mu_{(h_1,j)} \mid h_1=1,\ldots,\eta_j\}$ along the thickness direction. Among them, $\mu_{(h_1,j)}$ represents the total number of edge lines in the j-th cross-sectional area, and η_j-1 is the total number of yarn paths. The yarn path set is $\lambda'(j)=\{\mu'_{(h'_1,j)} \mid h'_1=1,\ldots,\eta_j-1\}$.

For the cross-sectional area with two boundary endpoints shown in Fig. 6, the "lower surface" segmentation method needs to be used. Firstly, extract the lower surface edge line $\varepsilon_{down(g_2,j)}$, and

calculate the normal vector $\overrightarrow{F_d}(j)$ of the flattening center point $\xi'_d(j)$. Translate the flattening center point $\xi'_d(j)$ along the normal vector direction by a distance of T_{yarn} for η_j times to obtain the segmentation reference point $\xi'_d(h_1, j)$. At the same time, translate the lower surface edge line along the segmentation reference point $\xi'_d(h_1, j)$ to obtain the intersection points $\zeta'_l(h_1, j)\{h_1 = 1, \ldots, \eta_j\}$ and $\zeta'_r(j, h_1)\{h_1 = 1, \ldots, \eta_j\}$ of the left and right ends of the lower surface edge line and the upper surface edge line, respectively. Finally, intercept the point set of the lower surface edge line in the $\{\zeta'_l(h_1, j), \ldots, \zeta 1(j)\}$ and $\{\zeta 1(j), \ldots, \zeta'_r(h_1, j)\}$ regions during the translation process to obtain the cross-sectional area segmentation set $\lambda(j)$ and the yarn path set $\lambda'(j)$.

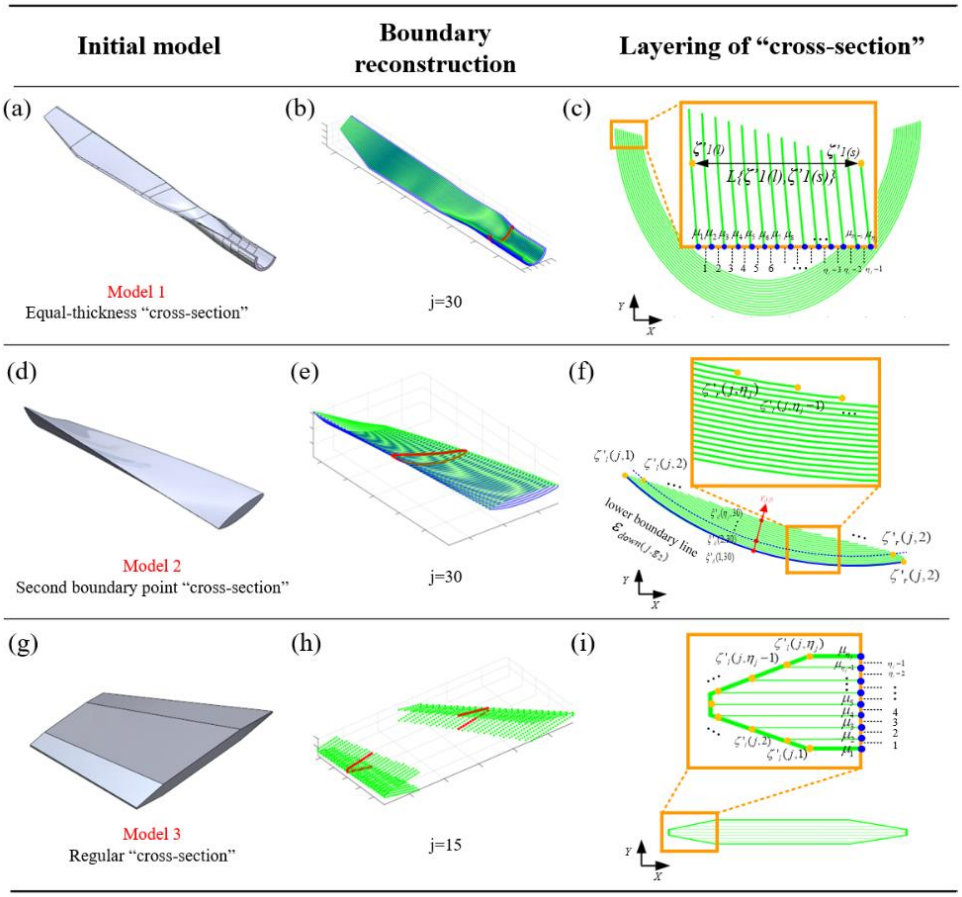


Fig. 6 Model with uniform thickness - Model 1: (a) Initial model, (b) Boundary reconstruction model, (c) Cross-sectional stratification at j=30. Model with two boundary points - Model 2: (d) Initial model, (e) Boundary reconstruction model, (f) Cross-sectional stratification at j=30. Regular Model - Model 3: (g) Initial model, (h) Boundary reconstruction, (i) Cross-sectional layering at j=15.

For the regular cross-sectional area shown in Fig. 6, a "top-to-bottom" step-by-step segmentation method is used. The intersection points of the segmentation line with the left and right boundaries of the cross-sectional area are $\zeta'_l(h_1)\{h_1=1,\ldots,\eta_j\}$ and $\zeta'_r(h_1)\{h_1=1,\ldots,\eta_j\}$, respectively. The set of the number of segmentation layers in the regular cross-sectional area type is $\lambda(j)=\{\zeta'_l(h_1,j),\zeta'_r(h_1,j)\}$, and the left and right endpoints are important parameters for designing the composite structure.

3.3 Extraction of Central Datum Line in Flattening Process

For the complex woven composite model shown in Fig. 6, the preform undergoes torsional deformation during the forming process. Therefore, the torsional deformation effect also needs to be considered when extracting the central datum points during the flattening process. As shown in Fig. 3, different flattening methods are selected for the central datum line extraction process according to the type of cross-sectional area, which mainly include constant thickness cross-sections (Model 1) and non-constant thickness cross-sections (Model 2). For the regular cross-sectional type components (Model 3), the central datum line is directly extracted as the central plane along the X-coordinate direction (Fig. 6), and the spatial information of the intersection points at the left and right ends during the layering process is important data of the model.

For components with constant thickness cross-sectional areas, it is first necessary to calculate their center line $\varepsilon_{center(j,g_2)}$ and the set of center points $\xi_c(j)$ of the center line based on the upper and lower boundary lines $\varepsilon_{up(j,g_2)}$ and $\varepsilon_{down(j,g_2)}$. The center point set $\xi_c(j)$ is fitted based on the warp width W_{warp} to obtain $\xi'_c(j)$ (Fig. 7(b)). The x-value of $\xi'_c(j)$ is used as the reference coordinate in the X-direction during the flattening process. As shown in Fig. 7(a), $\xi'_c(28)$ is used as the initial point of the cross-sectional area, and $\overrightarrow{F_c}(28)$ is the normal vector at point $\xi'_c(28)$, whose intersection points with the upper and lower edge lines are $\xi'_u(28)$ and $\xi'_d(28)$, respectively. Project this point and its normal vector along the Y-axis direction to the cross-sectional area at *j=29* to obtain $\xi'_c(29)$, $\overrightarrow{F_c}(29)$, and the intersection points $\xi'_u(29)$ and $\xi'_d(29)$ of $\overrightarrow{F_c}(29)$ with the upper and lower edge lines. Based on the judgment of the X-value when $\xi'_c(j)\{j=29,30\}$, it is known that its center point needs to be offset to the right by a distance equal to the warp width W_{warp}. That is, project $\xi'_c(29)$ along the Y-axis direction to the cross-sectional area at j=30 to obtain $\xi''_c(30)$. Then move $\xi''_c(30)$ along the arc until the moving distance is equal to the warp width W_{warp}, thereby obtaining $\xi'_c(30)$.

$$L\{\xi'_c(30),\xi''_c(30)\}=W_{warp} \tag{10}$$

For special-shaped components with cross-sectional areas with two boundary endpoints, the center point set $\xi_d(j)$ is the center of the lower edge line $\varepsilon_{down(g_2,j)}$. The center line point set $\xi_d(j)$ is fitted based on the warp width W_{warp} to obtain $\xi'_d(j)$ (Fig. 7(d)). The x-value of $\xi'_d(j)$ is used as the reference coordinate in the X-direction during the flattening process. As shown in Fig. 7(c), $\xi'_d(17)$ is used as the initial point of the cross-sectional area, and $\overrightarrow{F_d}(17)$ is the normal vector at point $\xi'_d(17)$, whose intersection point with the upper edge line is $\xi'_u(17)$. Similarly to the constant thickness cross-sectional area, based on the judgment of the X-value of $\xi'_c(j)\{j=18,19\}$, it is known that its center point needs to be offset to the left by a distance equal to the warp width W_{warp}. That is, project $\xi'_d(17)$ along the Y-axis direction to the cross-sectional area at j=18 to obtain $\xi'_d(18)$. Then move $\xi'_d(18)$ along the arc until the moving distance is equal to the warp width W_{warp}, thereby obtaining $\xi''_d(18)$.

$$L\{\xi'_d(18),\xi''_d(18)\}=W_{warp} \tag{11}$$

Fig. 7 shows the initial flattening datum lines, the flattening datum lines fitted by the warp width, and the flattening datum lines considering the torsion mapping effect for the constant thickness cross-section model and the non-constant thickness cross-section model, respectively. The red point set at the lower left of Fig. 7(b) is the intersection points of the normal vector at the center line of Model 1 with the upper and lower surfaces. The red point set at the lower left of Fig. 7(d) is the coordinates of the intersection point of the normal vector at the center point of the lower surface of Model 2 with the upper surface.

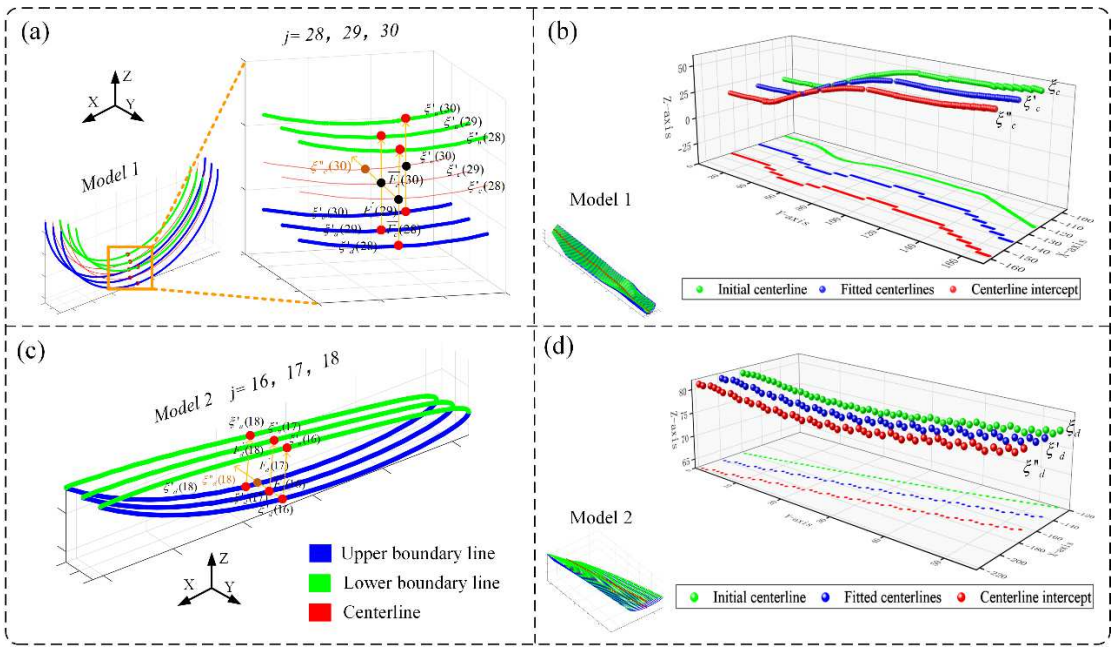


Fig. 7 Calculation methods of flattening datum points for different types of cross-sectional areas: (a) and (b) Model 1; (c) and (d) Model 2.

3.4 Construction of Yarn Path Point Model in Flattened State

The layering process of the cross-sectional area provides a data foundation for the yarn path point reconstruction process, and the extraction of the flattening reference line provides a reference benchmark for the yarn path point reconstruction process. The yarn path point reconstruction process is a process of predicting the initial position of the yarn path points of the preform based on the structural change characteristics of the composite material. Through this process, the composite material can be accurately decomposed in thickness, so as to facilitate the subsequent profiling design of the entire composite material.

3.4.1 Principle of Yarn Path Point Reconstruction

Yarn path point reconstruction is a key step in this paper based on the layered data of the cross-sectional area and the flattened central datum line. As shown in Fig. 8(a), there are two methods for reconstructing yarn path points symmetrically based on the central datum line. For reconstruction method 1, $\xi'_c(j)$ is the midpoint of the center line of the cross-sectional area, which is also a yarn path point, and $\overrightarrow{F_c}(j)$ is the normal vector at this point. $\overrightarrow{F_c}'(j)$ is the reference direction of the flattening process, with the direction vertically upward. The intersection points of the normal vector $\overrightarrow{F_c}(j)$ with each layer are $\xi'_c(h_1, j)$, and the central datum point of each layer during the flattening process is $\xi''_c(h_1, j)$. Taking $\xi'_c(h_1, j)$ as the central datum of $\mu'_{(h_1,j)}$, it is divided into left and right parts, and the arc lengths $L_l(h_1, j)$ and $L_r(h_1, j)$ at the left and right ends are extracted respectively. The number of yarn path points at the left and right ends is:

$$N_l(h_1, j) = \frac{L_l(h_1, j) - \frac{W_{warp}}{2}}{W_{warp}} = \frac{L_{\text{arc}}\{\zeta'_l(h_1, j), \ldots, \xi''_c(h_1, j)\} - \frac{W_{warp}}{2}}{W_{warp}} \tag{12}$$

$$N_r(h_1, j) = \frac{L_r(h_1, j) - \frac{W_{warp}}{2}}{W_{warp}} = \frac{L_{arc}\{\xi'_c(h_1, j), \ldots, \zeta''_r(h_1, j)\} - \frac{W_{warp}}{2}}{W_{warp}} \tag{13}$$

The initial yarn path point is $S'_{\text{Initial}} = \left\{P'_{(h_i,j,k_1)} = (u, v) \mid k_1 = 1, \ldots, N_l(h_1, j) + N_r(h_1, j) + 1\right\}$, and the yarn path point after flattening is $S''_{\text{Initial}} = \left\{P''_{(h_i,j,k_1)} = (u, v) \mid k_1 = 1, \ldots, N_l(h_1, j) + N_r(h_1, j) + 1\right\}$. For reconstruction method 2, the midpoint of the center line of the cross-sectional area is still $\xi'_c(j)$, but it is not a yarn path point. Similarly to reconstruction method 1, $\xi'_c(h_1, j)$ is used as the central datum of $\mu_{(h_1,j)}$, which is divided into left and right parts, and the arc lengths at the left and right ends are calculated respectively. The number of yarn path points at the left and right ends is:

$$N_l(h_1,j)=\frac{L_l(h_1,j)}{W_{warp}}=\frac{L_{arc}\{\zeta'_l(h_1,j),\ldots,\xi''_c(h_1,j)\}}{W_{warp}} \tag{14}$$

$$N_r(h_1,j)=\frac{L_r(h_1,j)}{W_{warp}}=\frac{L_{arc}\{\xi'_c(h_1,j),\ldots,\zeta''_r(h_1,j)\}}{W_{warp}} \tag{15}$$

The initial yarn path point is $S'_{\text{Initial}}=\left\{P'_{(h_i,j,k_1)}=(u,v)\,|\,k_1=1,\ldots,N_l(h_1,j)+N_r(h_1,j)\right\}$, and the yarn path point after flattening is $S''_{\text{Initial}}=\left\{P''_{(h_i,j,k_1)}=(u,v)\,|\,k_1=1,\ldots,N_l(h_1,j)+N_r(h_1,j)\right\}$.

As shown in Fig. 8(a), $\xi'_d(j)$ is the midpoint of the lower edge line $\varepsilon_{down(g_2,30)}$ of the cross-sectional area, where $\overrightarrow{F_d}(30)$ is the common normal vector of these two points. Similarly to the above, for reconstruction method 1 and method 2, the intersection points $\xi'_d(h_1,j)$ of $\overrightarrow{F_d}(30)$ with all layers are extracted respectively. Taking $\xi'_d(h_1,j)$ as the central datum for flattening each layer, the arc lengths $L_l(h_1,j)$ and $L_r(h_1,j)$ at the left and right ends of $\mu_{(h_1,j)}$, as well as the number of yarn path points $N_l(h_1,j)$ and $N_r(h_1,j)$ at the left and right ends, are calculated.

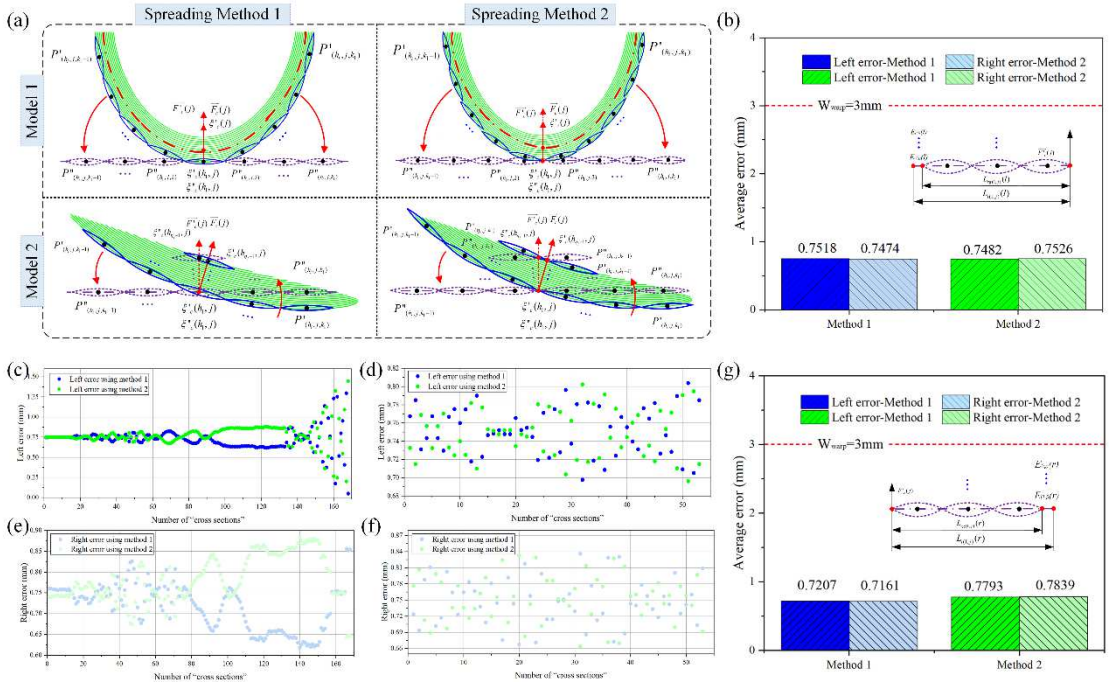


Fig. 8 (a) Two different yarn reconstruction methods: left-right symmetry and central symmetry. Reconstruction error distribution at the left and right ends under the two reconstruction methods: (c) and (e) Model 1; (d) and (f) Model 2. Average reconstruction error values at the left and right ends of the two reconstruction methods: (b) Model 1; (g) Model 2.

3.4.2 Evaluation of Reconstruction Correctness of Yarn Path Points

The interlacing point is the smallest unit in the 3D woven preform, and its parameters consist of the warp width and weft width. The smaller the interlacing point, the higher the profiling accuracy. In the structural design of 3D woven preforms, the smallest design unit is used to profile the structure of the component as much as possible. However, due to certain limitations of the smallest design unit itself, there is a certain profiling deviation in the yarn path point reconstruction process. The error calculation principle at the left and right ends during the yarn path reconstruction process and the average error value during the reconstruction process are shown in Fig. 8(b) and Fig. 8(g), respectively. Figs. 8(c)-(e) and Figs. 8(d)-(f) show the error distribution at the left and right ends of each cross-section during the reconstruction of Model 1 and Model 2, respectively. Interestingly, the reconstruction errors at the left and right ends of reconstruction method 1 and reconstruction method 2 both show a complementary trend.

4 Application and Results

In this study, a parameterized extraction method for the flattened yarn path point model of complex 3D woven composites was proposed. Sections 2 and 3 detailed the principle and process of this method, and the code for the above method was written using MATLAB software. To verify the wide applicability of this method, SolidWorks software was used to establish the composite model, and then the grid data was imported into MATLAB to implement the proposed method to generate the yarn path points of the flattened preform.

4.1 Flattened Yarn Path Point Models Under Different Composite Material Models

3D weaving technology is widely used in the field of composite materials, and 3D woven composites have various structural shapes, mainly including torsional deformation structures, regular structures, and composite structures of both. To verify the effectiveness of the proposed yarn path point reconstruction method in different composite material structures, this method was applied to various models, and the generated yarn path point models are shown in Fig. 9. Fig. 9(a) shows the model of a propeller blade. The structural characteristics of this model can be divided into three parts: a cylindrical region, a transition region, and a regular region, with large overall curvature changes. The propeller blade model was identified as a constant cross-section model during the cross-sectional area discrimination process. After layering and flattening it, a flattened yarn path point reconstruction model was obtained. Figs. 9(b)-(c) show the 3D woven composite blade models with torsional deformation. It can be seen from the left view and right view that the model has a large curvature deformation gradient. At the same time, during the molding process of the preform of such composites, the yarns will undergo large torsional deformation, so the design accuracy of its lower surface is very critical. In Section 4.3, the lower surface forming accuracy of the yarn path point reconstruction models of these two models was verified. Fig. 9(d) is a tail fin model, which has no torsional deformation, but its thickness along the radial and weft directions changes, leading to certain challenges in the overall thickness extraction and spatial distribution of the model. Through radial segmentation and vertical layering operations, a yarn path point reconstruction model was obtained, which can accurately reflect its thickness distribution law.

Therefore, the method proposed in this paper can generate a flattened yarn path point model. At the same time, since the generated path points correspond to the actual forming dimensions, this provides the possibility for the visualization of yarn reduction points, jacquard pattern design, and macro model construction during the weaving process, and lays a foundation for the finite element analysis of macro models of 3D woven composites with different structures.

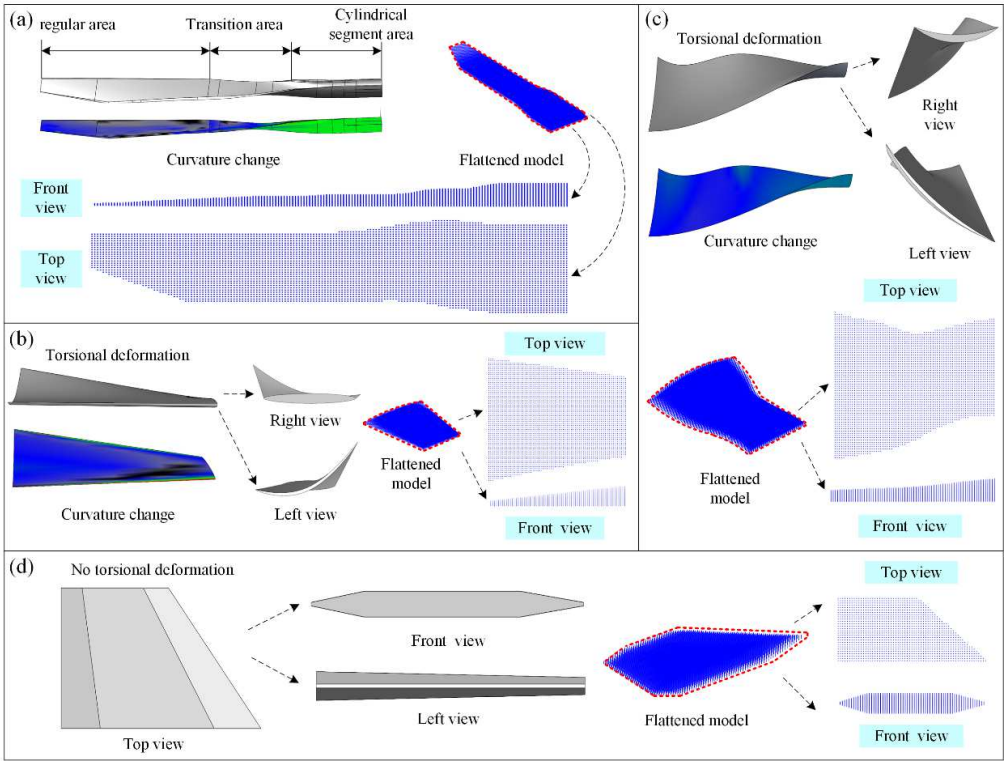


Fig. 9 Reconstruction models of yarn path points with different structures: (a) Structural model with multiple deformation modes; (b)-(c) Structural models with torsional deformation; (d) Regular and non-torsional deformation structural models.

4.2 Flattened Yarn Path Point Models Under Different Process Parameters

Different yarn specifications correspond to different dimensional parameters, which affect the process design parameters in the design process of 3D woven preforms. The basic parameters include: warp width, weft width, and yarn thickness. At the same time, the design process of 3D woven preforms also includes processes such as warp plying and weft plying, with various process design methods. To verify the efficiency of the proposed yarn path points under different structural parameters, this method was applied to different combinations of basic parameters, and the number distribution cloud maps of the yarn path points are shown in Figs. 10(a)-(e).

The test model is the composite blade model shown in Fig. 9(c). As shown in Fig. 10(a), the weft width is changed, and the total number of cutting layers along the warp direction under the same structural model is 74 and 124, respectively. Comparing Figs. 10(b) and (c), as well as Figs. 10(c) and (d), it can be seen that changing the warp width and weft width respectively, the number and size of forming pixels along the warp and weft directions change accordingly. If the designed smallest unit becomes larger, on the contrary, the design accuracy of the preform will decrease. Figs. 10(d) and (e) show that the yarn thickness changes with the same warp width and weft width. The contour of the thickness distribution cloud map is reduced and more obvious, which means that the gradient of the number of warp yarns in a single design unit becomes smaller, and the number of yarn path points in a single design unit also decreases. In summary, the yarn path reconstruction model is applicable to the design situations of different process parameters, providing convenience for the design of 3D woven composites with complex structures.

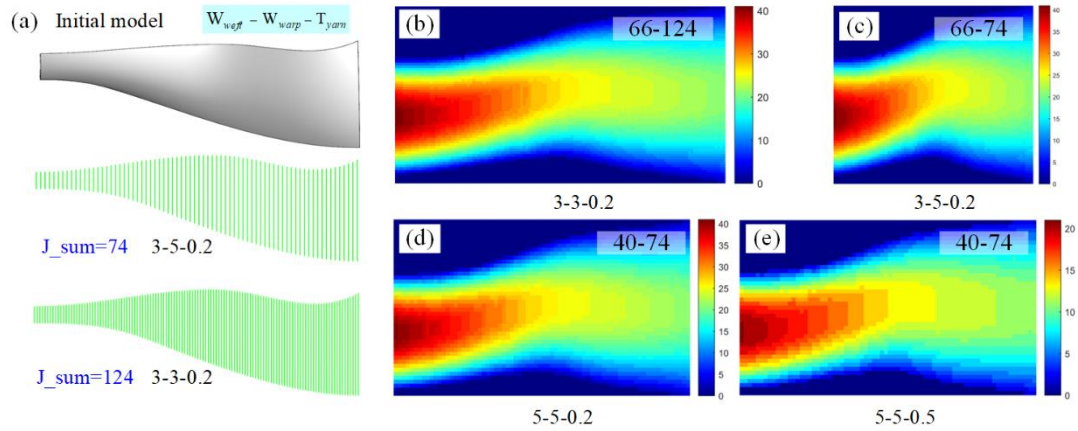


Fig. 10 (a) Number of cutting layers along the warp direction under different structural parameters. Distribution cloud maps of the number of yarn path reconstruction points under different structural parameters (warp width - weft width - yarn thickness): (b) 3mm-3mm-0.2mm; (c) 3mm-5mm-0.2mm; (d) 5mm-5mm-0.2mm; (e) 5mm-5mm-0.5mm.

4.3 Forming Accuracy Evaluation of 3D Woven Preforms

After the weaving of the 3D woven preform is completed, it is necessary to cut the shape of the preform. The accuracy of trajectory planning during the cutting process is a key step to ensure that the preform can be smoothly placed into the molding die and the composite material can be accurately formed. To verify the accuracy of the torsional effect of the proposed yarn path point reconstruction method, the lower surface of the yarn path point reconstruction model was extracted for a torsional deformation experiment. As shown in Fig. 11(a), first, the point cloud data of the lower surface of the flattened yarn path point reconstruction model was extracted, then the boundary point set of the lower surface was extracted, and finally, the path planning process during cutting was carried out based on the coordinate values of the boundary point set. The cutting material is a woven plain weave material, which is similar to the 3D woven material. During the forming process, the yarns will shift due to the influence of external forces. Fig. 11(b) shows the woven composite cutting machine and the cut woven plain weave material, respectively.

As shown in Fig. 11(c), the test models are the blade models with large torsional deformation shown in Figs. 9(b) and (c). During the mold design process, its upper surface was coincided with the lower surface of the initial model. Now, the cut woven plain weave composite material is laid in the designated mold. It is worth noting that the yarns of the laid plain weave material along the warp direction are twisted, and the yarns along the weft direction are depressed toward the bottom of the mold. As shown in Figs. 11(d) and (e), the plain weave woven material cut based on the lower surface boundary point data extracted by the yarn path reconstruction model proposed in this paper can well fit the molding die, which also verifies the correctness of the flattening process of the torsional deformation effect in the proposed method.

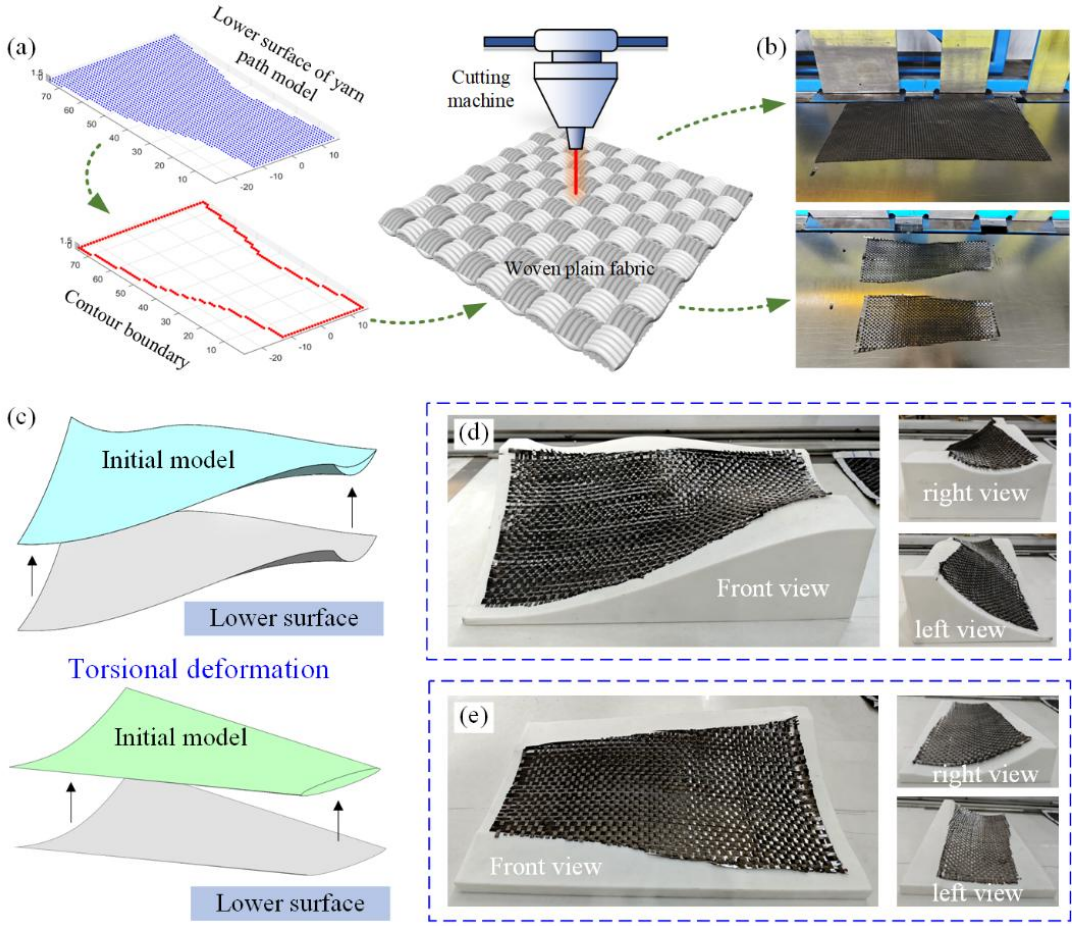


Fig. 11 (a) Boundary extraction of the yarn path point reconstruction model; (b) Cut woven plain weave fabric; (c) Lower surface extraction of the initial model. Forming accuracy verification of woven plain weave fabrics for different models: (d) Model 1; (e) Model 2.

5 Conclusions

This paper proposes a parameterized extraction method for the flattened yarn path point model of 3D woven composites with complex structures. The method optimizes and extracts cross-sectional areas along the warp direction and selects an adaptive layering method based on their types. In the process of extracting the flattening reference line, the mapping relationship between adjacent cross-sectional areas is considered, and the yarns in the cross-sectional areas are flattened based on the flattening reference line. The proposed yarn path point reconstruction method has significant advantages in predicting the thickness distribution of the flattened preform. Meanwhile, this method can also obtain the yarn path point distribution results of different complex structural models and structural parameters, realizing the visualization of the design of 3D woven preforms with complex structures. Finally, since the path points generated by the yarn path point reconstruction model correspond to the actual forming dimensions, the generated model provides a data foundation for the visualization of yarn reduction points and jacquard pattern design during the weaving process, which will be carried out in future work.

CRediT authorship contribution statement

Yinping Ye: Writing-original draft, Software, Methodology, Conceptualization. **Chengchang Ji:** Writing-review & editing, Supervision, Resources, Methodology, Conceptualization. **Xinfu Chi:**

Writing-review & editing, Supervision, Resources, Methodology, Conceptualization. **Yize Sun:** Resources.

Declaration of Competing Interest

The authors declare that they have no known competing financial interests or personal relationships that could have appeared to influence the work reported in this paper.

Acknowledgements

This work was supported by the Fundamental Research Funds for the Central Universities (grant numbers CUSF-DH-T-2024064), the Natural Science Foundation of Shanghai Basic Research Funding (25ZR1401011).

Data availability

Data will be made available on request.

References

[1] Liu G, Huang K, Zhong Y, et al. Investigation on the off-axis tensile failure behaviors of 3D woven composites through a coupled numerical-experimental approach[J]. Thin-walled structures, 2023, 192: 111176.

[2] Zhang J, Huang S, Gu B, et al. Fiber architecture effect on tensile and compressive damage mechanisms of 3D angle-interlock woven composites[J]. Composites Communications, 2023, 40: 101582.

[3] Qiao K, Xu X, Bui T Q, et al. A hierarchical coupled multiscale analysis for the tensile damage behavior of notched 3D woven composites[J]. Composite Structures, 2023, 306: 116611.

[4] Shah S Z H, Megat-Yusoff P S M, Karuppanan S, et al. Multiscale damage modelling of 3D woven composites under static and impact loads[J]. Composites Part A: Applied Science and Manufacturing, 2021, 151: 106659.

[5] Zhang C, Min L, Curiel-Sosa J L, et al. Ballistic performance and damage behavior of three-dimensional angle-interlock woven composites under high velocity impact: experimental and numerical studies[J]. Thin-Walled Structures, 2023, 191: 111056.

[6] Khatkar V, Behera B K, Manjunath R N. Textile structural composites for automotive leaf spring application[J]. Composites Part B: Engineering, 2020, 182: 107662.

[7] Carney K S, Pereira J M, Revilock D M, et al. Jet engine fan blade containment using an alternate geometry[J]. International journal of impact engineering, 2009, 36(5): 720-728.

[8] Huang T, Wang Y, Wang G. Review of the mechanical properties of a 3D woven composite and its applications[J]. Polymer-Plastics Technology and Engineering, 2018, 57(8): 740-756.

[9] Wei J, Zhang Y, Feng J, et al. Mechanical properties and failure mechanisms of 3D layer-to-layer interlock woven composites[J]. Polymer Composites.

[10] Majumdar A, Rathi A, Mawkhlieng U. Augmenting the mechanical performance of three-dimensional woven composites by the synergistic effect of fabric architecture and interfacial interaction of carbon nanotubes[J]. Polymer Composites, 2024, 45(3): 2629-2645.

[11] Coupe D, Dambrine B J G, Marlin F M P, et al. Method of manufacturing a gas turbine casing out of composite material, and a casing as obtained thereby: U.S. Patent 8,322,971[P]. 2012-12-4.

[12] Ekermann T, Stig F, Hallström S. Non-conformance aspects of moulded composite materials and “corresponding” simulation models with 3D textile reinforcement[J]. Composites Part A: Applied Science and Manufacturing, 2024, 186: 108367.

[13] Kim H, Park J. Improved modeling method for 3-dimensional woven composites using weaving parameters[J]. International Journal of Aeronautical and Space Sciences, 2021, 22: 824-833.

14] Gras R, Leclerc H, Hild F, et al. Identification of a set of macroscopic elastic parameters in a 3D woven composite: Uncertainty analysis and regularization[J]. International Journal of Solids and Structures, 2015, 55: 2-16.

[15] Dong L, Lekakou C, Bader M G. Processing of composites: simulations of the draping of fabrics with updated material behaviour law[J]. Journal of composite materials, 2001, 35(2): 138-163.

[16] Peng X Q, Cao J. A continuum mechanics-based non-orthogonal constitutive model for woven composite fabrics[J]. Composites part A: Applied Science and manufacturing, 2005, 36(6): 859-874.

[17] Badel P, Gauthier S, Vidal-Sallé E, et al. Rate constitutive equations for computational analyses of

textile composite reinforcement mechanical behaviour during forming[J]. Composites Part A: Applied Science and Manufacturing, 2009, 40(8): 997-1007.
[18] Charmetant A, Orliac J G, Vidal-Sallé E, et al. Hyperelastic model for large deformation analyses of 3D interlock composite preforms[J]. Composites Science and Technology, 2012, 72(12): 1352-1360.
[19] Mathieu S, Hamila N, Bouillon F, et al. Enhanced modeling of 3D composite preform deformations taking into account local fiber bending stiffness[J]. Composites Science and Technology, 2015, 117: 322-333.
[20] Pazmino J, Mathieu S, Carvelli V, et al. Numerical modelling of forming of a non-crimp 3D orthogonal weave E-glass composite reinforcement[J]. Composites Part A: Applied Science and Manufacturing, 2015, 72: 207-218.
[21] Naouar N, Vidal-Sallé E, Schneider J, et al. Meso-scale FE analyses of textile composite reinforcement deformation based on X-ray computed tomography[J]. Composite structures, 2014, 116: 165-176.
[22] Li M, Liu K, Ge J, et al. A novel modeling method for the mechanical behavior of 3D woven fabrics considering yarn distortion[J]. Composites Science and Technology, 2022, 230: 109691.
[23] Thompson A J, El Said B, Belnoue J P H, et al. Modelling process induced deformations in 0/90 non-crimp fabrics at the meso-scale[J]. Composites Science and Technology, 2018, 168: 104-110.
[24] Sirtautas J, Pickett A K, Lépicier P. A mesoscopic model for coupled drape-infusion simulation of biaxial Non-Crimp Fabric[J]. Composites Part B: Engineering, 2013, 47: 48-57.
[25] Wang J, Wang P, Hamila N, et al. Mesoscopic analyses of the draping of 3D woven composite reinforcements based on macroscopic simulations[J]. Composite Structures, 2020, 250: 112602.
[26] Bednarcyk B A, Stier B, Simon J W, et al. Meso-and micro-scale modeling of damage in plain weave composites[J]. Composite Structures, 2015, 121: 258-270.
[27] Sodhani D, Reese S, Jockenhövel S, et al. Multi-scale modelling and simulation of a highly deformable embedded biomedical textile mesh composite[J]. Composites Part B: Engineering, 2018, 143: 113-131.
[28] Li M, Li H, Ge J, et al. A hierarchical multi-scaling method for modeling the mesoscale geometry of 3D woven composite preform with twisted structure[J]. Composite Structures, 2025, 354: 118778.
[29] Gao X, Zhang X, Zhang S, et al. A parameterised and integrated modelling method for plain-weave composite preform of a component with complex geometry[J]. Composites Part A: Applied Science and Manufacturing, 2022, 154: 106748.
[30] Morioka K, Ohtake Y, Suzuki H, et al. 3D woven composite design using a flattening simulation[J]. Computer-Aided Design, 2016, 81: 24-38.